JOURNAL OF AIRCRAFT
Vol. 42, No. 5, September–October 2005

Ideal Aerodynamics of Ground Effect and Formation Flight

Rachel M. King* and Ashok Gopalarathnam†
North Carolina State University, Raleigh, North Carolina 27695-7910

The theoretical induced-drag benefits are presented for ideally loaded wings flying in formation and ground effect. An optimum-downwash approach using a vortex-lattice implementation was used to study formations of wings loaded optimally for minimum induced drag with roll trim. An exact approach was also developed to examine the drag of elliptically loaded wings in formation. The exact approach allows for decomposition of the benefits by considering the mutual-interference contributions from different pairs of wings in a formation. The results show that elliptically loaded wing formations have nearly the same drag as optimally loaded wing formations. For a formation of planar wings, in or out of ground effect, the optimum lateral separation corresponds to a 10% span overlap of wing tips. At this optimum lateral separation, a formation of 25 elliptically loaded wings flying out of ground effect experiences an 81% drag reduction compared to 25 wings flying in isolation. For large formations, in or out of ground effect, multiple local optima are seen for the lateral separation. Large formations experience small additional benefits caused by ground effect even at relatively large ground clearances of four wing spans. The shape of vee formations, for equipartition of drag benefits, is found to be nearly independent of flight in or out of ground effect.

Nomenclature

b	=	wing span of a single aircraft
b_{eff}	=	effective formation span
C_L	=	wing lift coefficient
C_l	=	section lift coefficient
c	=	local chord
D	=	induced drag
D_{ell}	=	induced drag of a single elliptically loaded wing out of ground effect
D_{ff}	=	interference drag caused by formation flight
D_{ge}	=	interference drag caused by ground proximity
D_{int}	=	mutual-interference drag for a pair of wings
$\boldsymbol{F}$	=	residual vector
f	=	index of the term for formation-flight interference drag
g	=	index of the term for ground-effect interference drag
h	=	height of wing above ground
$\boldsymbol{I}$	=	influence coefficient matrix of size $n \times n$
$\boldsymbol{J}$	=	Jacobain matrix
L	=	wing lift
l	=	winglet height
N	=	number of wings
n	=	number of horseshoe vortices on all of the wings
P, Q	=	constants used in defining normalwash distribution
R	=	wing rolling moment
r	=	function defining contribution of unit load to wing rolling moment, Eq. (3)
S	=	wing area
s	=	arc length along a wake trace of a wing
V_∞	=	freestream velocity
W	=	crossflow velocity distribution in the Trefftz plane
w	=	normalwash/downwash in the Trefftz plane
$\boldsymbol{w}$	=	vector containing the n Trefftz-plane normalwash values
w_0	=	Trefftz-plane downwash at midspan location on wing wake trace
$\bar{w}$	=	normalwash at quarter-chord
X	=	streamwise separation between adjacent wings
x	=	streamwise coordinate
Y	=	centerline-to-centerline lateral separation between adjacent wings
y	=	spanwise coordinate
Z	=	vertical separation between adjacent wings
$\mathcal{Z}$	=	complex coordinate in the Trefftz plane
z	=	vertical coordinate
Γ	=	bound-vorticity strength
$\boldsymbol{\Gamma}$	=	vector of the n bound-vortex strengths
γ	=	elemental area of additional bound vorticity
$\delta\boldsymbol{x}$	=	vector containing streamwise-position corrections
θ	=	local dihedral angle
ρ	=	density of air
σ	=	total induced drag of N-wing formation/ND_{ell}

Subscripts

A	=	wing A
av	=	average
B	=	wing B
m	=	mirrored image
2	=	two-wing formation

Superscripts

l	=	left wing tip
m	=	centerline of aircraft
r	=	right wing tip

Introduction

IT is well known that many species of migrating birds fly together in formations for improved aerodynamic efficiency. This improved efficiency results from the upwash generated by the wings of the neighboring birds. Some of the earliest quantitative estimates of the aerodynamic benefits of formation flight were presented by Wieselsberger,[1] who suggested that a vee-formation shape results in equal distribution of the drag benefits among all of the birds in a formation. The analytical study of Lissaman and Shollenberger[2] showed that a formation of 25 birds, flying with zero lateral spacing between wing tips, would have a 70% increase in range when compared to a lone bird. Similar benefits have been shown by other

Presented as Paper 2004-0906 at the AIAA 42nd Aerospace Sciences Meeting and Exhibit, Reno, NV, 5–8 January 2004; received 17 May 2004; revision received 30 September 2004; accepted for publication 14 October 2004.

*Graduate Research Assistant, Box 7910, Department of Mechanical and Aerospace Engineering; rmking2@eos.ncsu.edu. Student Member AIAA.

†Assistant Professor, Box 7910, Department of Mechanical and Aerospace Engineering; ashok_g@ncsu.edu. Senior Member AIAA.

researchers, including Hummel[3–5] and Hainsworth.[6] Recent in-flight measurements of heart beat rates of eight trained pelicans flying in formation and in isolation show that energy expenditure is reduced by nearly 14.5% when flying in formation,[7] clearly demonstrating the benefits.

Certain species of birds, such as pelicans, can often be seen flying either solo or in formation low above the water in ground effect.[8] It is well known from theoretical[9–13] and experimental studies[14–16] that flight in ground effect results in a reduction in the induced drag, an increase in the lift-curve slope, and an increase in the lift-to-drag ratio. It is believed that by flying close to the ground or water, birds such as the pelican are able to cover larger distances with less effort.[17]

The concepts of formation flight and flight in ground effect have the potential for application to aircraft, and each has been studied extensively by past researchers. The advantages and issues related to aircraft formation flight have been studied analytically,[5,18–21] in wind-tunnel experiments,[22,23] and in flight tests.[19,24–26] Research studies of aircraft flight in ground effect are detailed in a comprehensive literature survey by Rozhdestvensky,[12] which includes several aircraft concepts designed to exploit the advantages of ground-effect flight. Many early prototypes of such aircraft first originated in Russia, where they were designed and flight tested. A more recent design concept of a flight-in-ground-effect aircraft is the Boeing Pelican.[27] Past theoretical aerodynamic studies include the development of approaches for determining the optimum lift distributions and associated minimum induced drag values for formation flight,[20,21,28] ground-effect flight,[10,11,28] and combined ground-effect and formation flight.[29] These methods have typically used Lagrange-multiplier-based constrained-minimization approaches[18,30,31] or optimum-downwash[21] approaches implemented using vortex-lattice formulations, or were developed using exact solutions.[11]

Significant issues in maintaining proper aircraft position, either within a formation or close to the ground, however, have prevented the widespread use of formation flight and ground-effect flight as drag-reduction techniques. In addition, unlike the wings of birds, the rigid wings of current aircraft have limited capability for adapting the geometry to achieve ideal lift distributions that maximize the benefits of formation or ground-effect flight. Advances in precision measurement and control of relative position of aircraft and the development of adaptive-wing technology[32,33] have renewed the interest[27,28,34,35] in exploring the use of formation flight and ground-effect flight for achieving revolutionary improvements in aircraft aerodynamic efficiency.

Although previous investigations have studied the benefits of formation flight[1–5,19,22–26] and ground effect,[10–16] the benefits of combined formation and ground-effect flight have not received much attention even though migrating birds are known to fly in formation close to the water surface.[8] An exception is the work of McMasters and McLean,[29] in which an analytical study was used to propose that two human-powered aircraft flying in formation close to the water could successfully complete the flight across the English Channel for the £100,000 Kremer prize,[36] which was subsequently won by the flight of the Gossamer Albatross.[36,37] The main objective of the current research was to examine the aerodynamic benefits of combined ground effect and formation flight. For this purpose, optimally loaded planar and nonplanar wings, as well as elliptically loaded planar wings, were examined in order to determine the lower limit in induced drag attainable for any given formation and ground-effect geometry. In the current study, the optimum-downwash approach of Frazier and Gopalarathnam[21] was used for the study of optimally loaded wings, and exact solutions were developed for the study of elliptically loaded wings. Specific attention was paid to the effect of lateral separation and to the favorable/adverse interference effects between different pairs of wings in formation and ground-effect configurations.

Methodology

Optimum Lift Distribution for Minimum Induced Drag

To determine the optimum lift distribution on multiple wings in formation with constraints on the lift and zero rolling moment

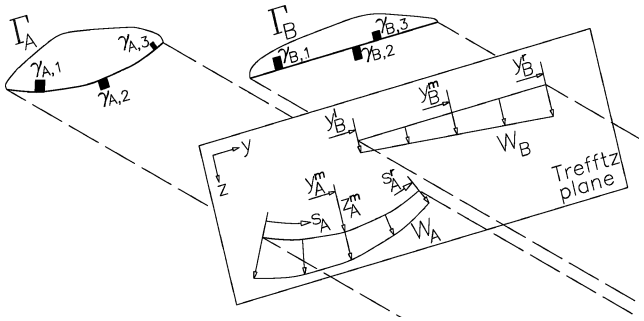

Fig. 1 Illustration of the loading and Trefftz-plane normalwash for the two-wing example.

on each wing, the methodology of Frazier and Gopalarathnam[21] was used. The methodology was extended in the current work to handle nonplanar wings, each with an arbitrary spanwise variation of dihedral. Only the essential elements of this methodology and the extension to nonplanar wings are described in this paper. For further details, the reader is referred to Ref. 21. In this method, the calculus-of-variation approach of Jones[38] is first used to determine the optimum downwash behind the wings. The wake is assumed to be rigid, inviscid, and invariant with the streamwise direction, and it is assumed to trail behind the wings in the direction of the freestream. Figure 1 is an illustration of an example two-wing formation, where A is a nonplanar wing with spanwise curvature, while B is a planar wing. The wings need not be identical, but both are assumed to be optimally loaded. The lift distributions on the two wings are such that the total induced drag of the formation is a minimum, and the total lift on each wing equals the corresponding weight while the rolling moment for each wing is zero. The position along the curved wing A is denoted using the arc length s_A, and the local dihedral angle at any spanwise location is $\theta_A(s_A)$. $\Gamma_A(s_A)$ and $\Gamma_B(s_B)$ are the bound-vorticity distributions associated with the original lift distributions on the two wings A and B. The lift L_A and L_B on each wing can be computed by spanwise integration, as shown in Eq. (1) for wing A:

$$L_A = \rho V_\infty \int_0^{s_A^r} \Gamma_A(s_A) \cos[\theta_A(s_A)]\, \mathrm{d}s_A \tag{1}$$

The wing rolling moment R as a result of the lift distribution can also be computed from the Γ distribution and is shown in Eq. (2) for wing A. The function $r_A(s_A)$, shown in Eq. (3), is the contribution to the rolling moment as a result of a unit load, acting normal to the curved wing, at s_A.

$$R_A = -\rho V_\infty \int_0^{s_A^r} \Gamma_A(s_A) r_A(s_A)\, \mathrm{d}s_A \tag{2}$$

$$r_A(s_A) = \cos[\theta_A(s_A)]\left[y_A(s_A) - y_A^m\right] - \sin[\theta_A(s_A)]\left[z_A(s_A) - z_A^m\right] \tag{3}$$

Using the Trefftz-plane normalwash distributions $w_A(s_A)$ and $w_B(s_B)$ shown in Fig. 1, the total induced drag of the entire formation with this lift distribution can be computed as shown in Eq. (4):

$$D = \frac{\rho}{2} \int_0^{s_A^r} w_A(s_A)\Gamma_A(s_A)\, \mathrm{d}s_A + \frac{\rho}{2} \int_0^{s_B^r} w_B(s_B)\Gamma_B(s_B)\, \mathrm{d}s_B \tag{4}$$

As pointed out in Ref. 20, the induced drag for each individual wing cannot be determined using the Trefftz-plane normalwash and has to be computed using a near-field method. Using wing A as an example, suppose the lift distribution on the wing is modeled using a bound vortex of varying strength $\Gamma_A(s_A)$ along the quarter-chord line and $\bar{w}_A(s_A)$ is the normalwash distribution along this line, then

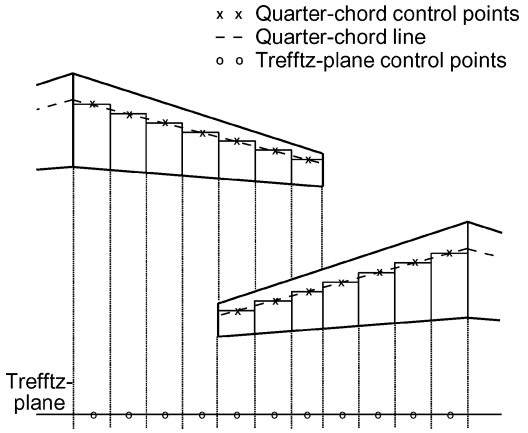

Fig. 2 Illustration of vortex-lattice arrangement for a pair of swept wings.

the induced drag of wing A is

$$D_A = \rho \int_0^{s_A^r} \bar{w}_A(s_A)\Gamma_A(s_A)\,\mathrm{d}s_A \tag{5}$$

It was shown by Iglesias and Mason[20] that when using a vortex lattice method (VLM), the bound vortex leg of each horseshoe vortex needs to be unswept in order for the total near-field induced drag value from Eq. (5) to match that computed from the far-field integration using Eq. (4). For this reason, the bound-vortex legs in the VLM formulation for the current work are unswept, as illustrated in Fig. 2. In addition, when modeling multiple lifting surfaces with overlapping wake traces using the VLM, care was taken in the current work to ensure that the overlapping trailing-vortex legs of the wings were exactly aligned, as shown in Fig. 2.

The goal of the current method is to determine the downwash distribution behind the wings that will result in a minimum for the total induced drag of the entire system of wings while satisfying the constraints on the desired lift and desired zero rolling moment on each wing. As presented by Jones,[38] if the original lift distribution results in minimum induced drag, then a small variation in the shape of the lift distribution will produce no first-order change. For such an original lift distribution, the drag arising from the small additional Γ distribution acting on the original Trefftz-plane normalwash distribution will be zero, as shown in greater detail in Ref. 21.

To satisfy the constraints on the specified lift and zero rolling moment, the additional Γ distribution should be selected such that it generates no additional lift or rolling moment for each wing. This additional Γ distribution is shown in Fig. 1 along with the original Γ distribution for the two wings. Using the arguments of Jones,[38] any additional distribution meeting these requirements can be subdivided into groups of three elements, so that each individual group independently satisfies the constraints. For instance, wing A has an additional distribution, which is composed of three elements having areas $\gamma_{A,1}$, $\gamma_{A,2}$, and $\gamma_{A,3}$, and are arbitrarily located at $s_{A,1}$, $s_{A,2}$, and $s_{A,3}$ respectively, as seen in Fig. 1. The additional Γ distribution must satisfy the following conditions: 1) there should be no change in the lift on wings A and B [Eqs. (6) and (7)], 2) there should be no change in the rolling moments [Eqs. (8) and (9)], and 3) there should be no change in the total induced drag [Eq. (10)]. In Eq. (10), $w_{A,1}$, $w_{A,2}$, and similar terms are the Trefftz-plane normalwash values associated with the original Γ distribution at the corresponding locations $s_{A,1}$, $s_{A,2}$, and so on.

$$\gamma_{A,1}\cos[\theta_A(s_{A,1})] + \gamma_{A,2}\cos[\theta_A(s_{A,2})] + \gamma_{A,3}\cos[\theta_A(s_{A,3})] = 0 \tag{6}$$

$$\gamma_{B,1}\cos[\theta_B(s_{B,1})] + \gamma_{B,2}\cos[\theta_B(s_{B,2})] + \gamma_{B,3}\cos[\theta_B(s_{B,3})] = 0 \tag{7}$$

$$\gamma_{A,1}r_A(s_{A,1}) + \gamma_{A,2}r_A(s_{A,2}) + \gamma_{A,3}r_A(s_{A,3}) = 0 \tag{8}$$

$$\gamma_{B,1}r_B(s_{B,1}) + \gamma_{B,2}r_B(s_{B,2}) + \gamma_{B,3}r_B(s_{B,3}) = 0 \tag{9}$$

$$\gamma_{A,1}w_{A,1} + \gamma_{A,2}w_{A,2} + \gamma_{A,3}w_{A,3} + \gamma_{B,1}w_{B,1} + \gamma_{B,2}w_{B,2} + \gamma_{B,3}w_{B,3} = 0 \tag{10}$$

To satisfy Eqs. (6–10), the Trefftz-plane normalwash along the wake traces of each wing must be of the form $w_A(s_A) = P_A\cos[\theta_A(s_A)] + Q_A r_A(s_A)$ and $w_B(s_B) = P_B\cos[\theta_B(s_B)] + Q_B r_B(s_B)$, where P_A, Q_A, P_B, and Q_B are constants that are determined using the specified values of the lift, L_A and L_B, and the rolling moments, R_A and R_B, for the two wings. In the current problem, R_A and R_B are both zero. For a planar wing ($\theta = 0$), this normalwash variation simplifies to a linear spanwise variation[21] of the downwash distribution, $w_B(y) = P_B + Q_B(y - y_B^m)$, as illustrated for wing B in Fig. 1. Although this method has been illustrated using two wings, the result can be generalized for any arbitrary number of wings in formation flight.

The optimum-downwash formulation for planar wings is valid only for formation geometries in which the wake traces of the wings in the Trefftz plane do not intersect or overlap with each other. If any two planar wings have intersecting or overlapping wake traces, then they share the same Trefftz-plane downwash values at each of the common points of overlap. Because the formulation does not account for such a constraint in the downwash, the method is restricted to wings that do not intersect or overlap in the front view. This limitation is also applicable to the constrained-minimization approach of Ref. 20.

The Γ distributions on the wings and the associated Trefftz-plane normalwash distributions w behind them are closely related and can be determined using a discrete-vortex method similar to that described by Blackwell,[39] as detailed in Ref. 21. For a given formation of several wings with the geometry specified in the front view, and known values for the specified lift and zero rolling moments, the approach allows for the computation of the values of P and Q that in turn determine the Trefftz-plane normalwash. The Γ distributions are then computed, from which other quantities can be determined. If, in addition, the planform geometry of the entire formation is known, the induced drag for each individual wing can also be computed using the near-field approach[20] shown in Eq. (5) for wing A.

Ground Effect

For analysis of a single wing or a formation of several wings in ground effect, an additional formation is modeled as a mirror image under the ground plane. The wings in the mirrored formation are specified to have values of lift that are negative and equal to those specified for the corresponding wings in the upper formation, as illustrated in Fig. 3 for a two-wing formation in ground effect. As an example, for wing A in ground effect, at a height above ground of h_A, the wing mirrored underneath, designated A_m, would have the desired value of lift $L_{Am} = -L_A$. The desired rolling moments, R_A and R_{Am}, remain zero. Beyond these changes, the formulation

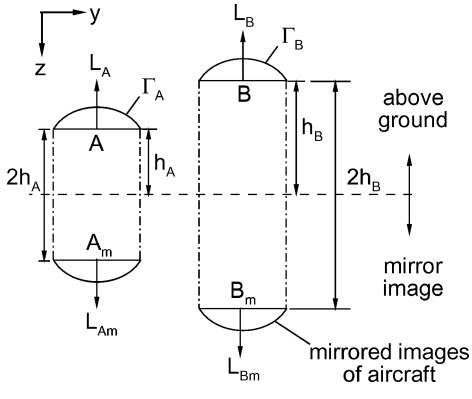

Fig. 3 Model of two-wing formation in ground effect.

for calculating the optimum normalwash and lift distributions remains the same as that presented for flight out of ground effect. In the vortex-lattice implementation, lateral symmetry as well as symmetry about the ground plane are used to significantly reduce the computational time using standard techniques.[13]

Prescribed Elliptical Lift Distribution

Whereas the optimum lift distribution for a given formation results in the minimum total induced drag, it is desirable to determine how sensitive the induced drag is to deviations of the lift distribution from the optimum distribution. For this purpose, formations of planar wings were also examined in which each wing was assumed to have an elliptical spanwise lift distribution. When an elliptical loading is prescribed, the wing rolling-moment constraint is automatically satisfied. Prescription of an elliptical loading also enables the investigation of formation geometries with overlapping wings, which is not feasible with optimally loaded wings. More importantly, the exact solution for the crossflow velocity in the Trefftz plane is known for an elliptically loaded wing. This crossflow velocity can be used to obtain the exact solution for the total drag of a formation of several wings flying in ground effect (IGE) or out of ground effect (OGE). The exact solution can also serve to validate the vortex-lattice solutions for elliptically loaded wings.

For a wing with its plane of symmetry located at y^m, the prescribed elliptical lift distribution results in an elliptical Γ distribution over the span as follows:

$$\Gamma(y, y^m)\big/V_\infty = (\Gamma_0/V_\infty)\sqrt{1-[2(y-y^m)/b]^2} \qquad (11)$$

where

$$\frac{\Gamma_0}{V_\infty} = \frac{4L}{\pi\rho b V_\infty^2} = \frac{2SC_L}{\pi b} \qquad (12)$$

When using the vortex-lattice implementation, the vortex strengths are determined from the elliptical loading of lift on each wing. These vortex strengths are used to compute the resulting Trefftz-plane downwash, the induced drag of the formation [Eq. (4)], and induced drag values of individual wings [Eq. (5)]. For a single elliptically loaded wing operating out of ground effect, lifting-line theory gives the induced drag to be

$$D_{\text{ell}} = \left(2\big/\pi\rho V_\infty^2\right)(L/b)^2 \qquad (13)$$

The exact solution for the crossflow velocity distribution in the Trefftz plane, expressed using complex variables, is[40,41]

$$W(y,z)/V_\infty = (v-iw)/V_\infty$$
$$= i(w_0/V_\infty)\left[\mathcal{Z}\big/\sqrt{\mathcal{Z}^2-(b/2)^2}-1\right] \qquad (14)$$

where $\mathcal{Z} = y + iz$ is the complex coordinate in the Trefftz plane with the origin at the midspan location of the wake trace of the wing. The Trefftz-plane downwash at the midspan location on the wake trace w_0 is given by

$$\frac{w_0}{V_\infty} = \frac{4L}{\pi\rho V_\infty^2 b^2} = \frac{2C_L}{\pi AR} \qquad (15)$$

The downwash w and the vertical coordinate z are assumed to be positive in the downward direction. For planar wings, only the downwash component of $W(y, z)$ is of interest and is given by

$$w(y,z)/V_\infty = (w_0/V_\infty)\Re\left[1-\mathcal{Z}\big/\sqrt{\mathcal{Z}^2-(b/2)^2}\right] \qquad (16)$$

where the symbol $\Re$ denotes the real part of a complex variable. Figure 4 shows the variations of $w(y/b)/w_0$ for various values of z/b. It can be seen that for $z=0$ the downwash is constant over the span and there is upwash outboard of the wing tip. Immediately outboard of the wing tip, there is a singularity as the upwash goes to infinity. As a result of this singularity, evaluation of the induced drag for overlapping wings needs to be done carefully.

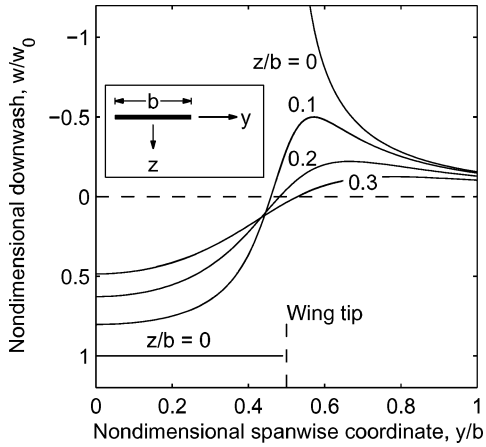

Fig. 4 Variation with *y/b* for various *z/b* of the downwash in the Trefftz plane for an elliptically loaded wing. Inset shows wake trace and coordinate system.

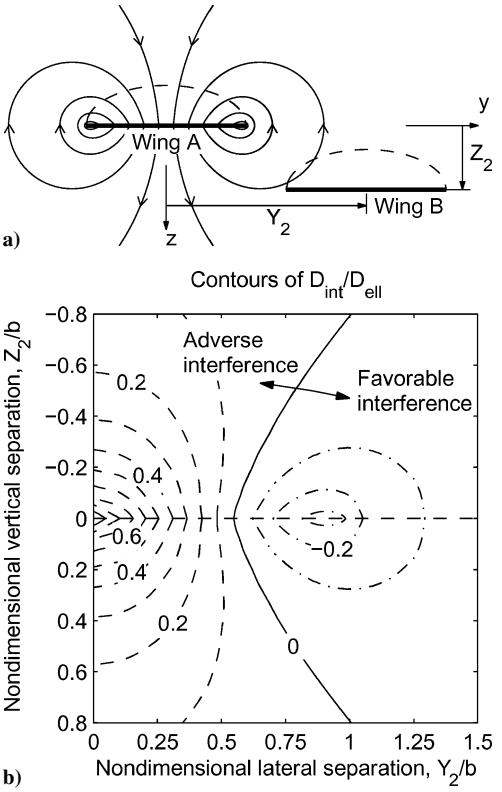

Fig. 5 Two elliptically loaded wings A and B: a) illustration of the wake-trace geometry, with the streamlines shown for wing A and b) contours of $D_{\text{int}}/D_{\text{ell}}$ as a function of Y_2/b and Z_2/b.

For a formation of several elliptically loaded wings of equal span and lift, in or out of ground effect, the exact solution for the total induced drag can be developed using the interference drag of a two-wing formation. This two-wing interference drag can be obtained in a manner similar to that for Prandtl's biplane theory.[42] Figure 5a shows two elliptically loaded wings, A and B, which have the same span and lift. The streamlines of the Trefftz-plane crossflow velocity distribution $W(y, z)$ of wing A are also plotted in Fig. 5a for reference. The total induced drag $D_2(Y_2, Z_2)$ for the two-wing formation as a function of the lateral separation Y_2 and vertical separation Z_2 and can be written as the sum of the self-induced contributions D_{AA} and D_{BB} and the mutual-interference contributions D_{AB} and D_{BA}. Each self-induced drag term is equal to the drag of a single elliptically loaded wing D_{ell}. The two mutual interference contributions

D_{AB} and D_{BA} are equal and are denoted by D_{int}.

$$D_2(Y_2, Z_2) = 2D_{ell} + 2D_{int}(Y_2, Z_2) \tag{17}$$

The self-induced drag terms can be determined using Eq. (13), and the mutual-interference term D_{int} can be computed for cases with nonoverlapping wake traces by integrating over the wake trace of wing B as follows:

$$D_{int}(Y_2, Z_2) = \frac{\rho}{2} \int_{Y_2 - b/2}^{Y_2 + b/2} w_A(y, Z_2)\Gamma_B(y, Y_2)\, \mathrm{d}y \tag{18}$$

where Γ_B is the bound circulation distribution on wing B obtained by setting $y_m = Y_2$ in Eq. (11) and w_A is the downwash distribution caused by wing A obtained by setting $z = Z_2$ in Eq. (14). For cases with overlapping wake traces ($Z_2 = 0$ and $0 < Y_2 < b$), the singularity of infinite upwash in w_A just outboard of the wing tip was handled by evaluating the Cauchy principal value at the singularity as follows:

$$D_{int}(Y_2, Z_2) = \frac{\rho}{2} \lim_{\epsilon \to 0} \left(\int_{Y_2 - b/2}^{b/2 - \epsilon} w_A \Gamma_B \, \mathrm{d}y + \int_{b/2 + \epsilon}^{Y_2 + b/2} w_A \Gamma_B \, \mathrm{d}y \right) \tag{19}$$

The expressions for Eqs. (18) and (19) were solved using the MATLAB® Symbolic Toolbox.[43] It can be shown that the nondimensional interference drag D_{int}/D_{ell} is a function of only the nondimensional lateral separation Y_2/b and vertical separation Z_2/b. Figure 5b shows the contours of D_{int}/D_{ell} as a function of Y_2/b and Z_2/b. Negative D_{int} is termed "favorable interference" as it results in a lower total drag for the formation, while positive D_{int} is considered "adverse interference." When wing A has positive lift and wing B has negative lift, as it would be if B were the mirror image of another wing flying close to the ground, then the interference drag between A and B would have the same magnitude, but would change sign. Therefore, regions of favorable interference become adverse interference and vice versa when wings A and B have lift acting in opposite directions.

It can be seen from Fig. 5b that the favorable interference is maximum at $Z_2/b = 0$ and $Y_2/b = 0.91$. That is, the maximum favorable interference occurs when the two wings have a small lateral overlap of approximately 9% of the wing span. When there is lateral overlap, the extreme-left portion of wing B that is overlapped laterally with wing A will experience the Trefftz-plane downwash of wing A. This downwash acting on the Γ of the overlapped portion of wing B will contribute to an increase in total induced drag. However, the spanwise portion of wing B that is just outboard of wing A will experience the significant Trefftz-plane upwash of wing A. This upwash acting on the Γ of the portion of wing B that is just outboard of wing A will contribute to a decrease in the total induced drag. These two contributions change with changes to the lateral separation, such that the small lateral overlap of 9% span results in maximum favorable interference.

To demonstrate how the two-wing interference-drag solution can be used to determine the total induced drag of several wings flying in formation, IGE or OGE, a formation of N elliptically loaded wings, numbered 1 to N, is considered. For the case of combined formation and ground-effect flight, the total formation drag can be written as

$$D = \sum_{j=1}^{N} \sum_{i=1}^{N} D_{ij} + \sum_{j=1}^{N} \sum_{i=1}^{N} D_{i(j_m)} \tag{20}$$

The first term of Eq. (20) provides the total drag of the formation when flying OGE. When $i = j$, D_{ij} is equal to D_{ell}. The second term provides the additional contribution caused by ground effect, with $D_{i(j_m)}$ being the induced drag caused by the downwash field of the image j_m of wing j acting on the wing i. It is also seen that each of the terms of D_{ij} and $D_{i(j_m)}$ can be computed using the two-wing interference-drag solution $D_{int}(Y_2, Z_2)$. For the special case of a formation of N elliptically loaded planar wings that are flying with uniform lateral separation between any two adjacent wings, zero vertical separation, and close to the ground, the total induced drag can be written as

$$D = ND_{ell} + D_{ff} + D_{ge} \tag{21}$$

where D_{ff} is the interference drag of the entire formation OGE and D_{ge} is the interference drag caused by ground proximity. D_{ff} can be written as

$$D_{ff} = \sum_{f=1}^{(N-1)} 2f D_{int}[(N - f)Y, 0] \tag{22}$$

where Y is the uniform lateral spacing between any two adjacent wings in the formation, with zero vertical separation. D_{ge} can be written as

$$D_{ge} = -ND_{int}(0, 2h) - \sum_{g=1}^{(N-1)} 2g D_{int}[(N - g)Y, 2h] \tag{23}$$

This formulation allows for the decomposition of the total induced drag into different contributions. In Eq. (22), the term for $f = N - 1$ represents the contributions of the interference drag between the $N - 1$ pairs of adjacent wings (wings i and $i + 1$), the term for $f = N - 2$ represents the contributions of the interference drag between the $N - 2$ pairs formed by a wing and its next-to-immediate neighbor (wings i and $i + 2$), and so on. Similarly in Eq. (23), the first term represents the N contributions of the interference drag between a wing and its own image, the $g = N - 1$ represents the $N - 1$ contributions of the interference drag between a wing and the image of its adjacent neighbor (wings i and image of $i + 1$), and so on. As shown later, this decomposition makes it possible to explain certain patterns in the variation of drag with lateral spacing and ground height. Finally, this exact formulation can only provide the total induced drag and cannot provide the drag of each individual in a formation. When the drag of each individual is needed, the vortex-lattice implementation is used.

Optimum Vee-Formation Shape

It is well known that a number of species of migrating birds such as swan, geese, and cranes fly in typical vee-shaped formations. This flight mode is shown to result in an aerodynamic benefit for all individuals.[1–4] From Munk's stagger theorem,[44] any lifting assemblage can be staggered, or displaced in the direction of motion, without changing the total induced drag. To determine optimal vee formations, a Newton iteration scheme was developed to determine the streamwise locations that result in equal induced drag for all of the individuals. At each step of the Newton iteration, the matrix equation

$$\boldsymbol{J} \cdot \delta \boldsymbol{x} = -\boldsymbol{F} \tag{24}$$

is solved. In this equation, $\boldsymbol{F}$ is the vector containing the residuals of the functions to be zeroed, $\boldsymbol{J}$ is the Jacobian matrix that contains the gradient information, and $\delta \boldsymbol{x}$ contains the corrections to the design variables causing $\boldsymbol{F}$ to approach zero. The target-induced drag for each individual $(D_i)_{target}$ is simply the total induced drag of the formation calculated in the Trefftz plane divided by the total number of wings N. The residual vector $\boldsymbol{F}$ is the difference between the current induced drag for each wing, determined using the vortex-lattice implementation, and the $(D_i)_{target}$. The Jacobian matrix contains the partial derivatives of the values of individual induced drag with respect to the streamwise locations of the wings and is determined using finite differencing. More details and equations for the procedure are provided in Ref. 45.

For each iteration, the matrix equation, Eq. (24), is solved to determine the vector $\delta \boldsymbol{x}$, as $\boldsymbol{J}$ and $\boldsymbol{F}$ are known. The resulting vector $\delta \boldsymbol{x}$, containing the corrections to the streamwise locations of the wings, is used for updating the shape of the vee formation. It was necessary to add an underrelaxation factor of 0.1 to make the iteration converge. That is, the x location for wing j is updated as

$x_j^{\text{new}} = x_j^{\text{old}} + (0.1)\delta x_j$. New individual D_i values are then calculated using the updated streamwise locations, and the residuals and Jacobian matrix are recalculated. This process is continued until the residuals are brought to within a given tolerance of zero, resulting in the streamwise locations for an optimum vee formation.

Validation of Optimum-Loading Method

This section presents a comparison of induced drag computed from the current optimum-loading VLM with exact solutions for wing formations IGE and OGE.

Planar Wing out of Ground Effect

From classical lifting-line theory, the exact optimum lift distribution for a single planar wing flying OGE is an elliptical loading, and the corresponding minimum induced drag is D_{ell}. Figure 6a shows a comparison of the lift distribution from the current method with the exact elliptical loading. The comparison is seen to be excellent. Figure 6b shows the convergence of the induced drag from the current method with increasing number of vortex lattices. It can be seen that the predicted drag converges toward the exact value with increasing number of lattices. For the current work, 80 lattices per half-span of each wing have been used for all vortex-lattice computations in order to achieve a reasonable compromise between accuracy and computation time for the larger formation geometries.

The optimum loading for minimum induced drag was also computed for a symmetric formation of three wings and was compared with the results from the constrained-minimization approach of Iglesias and Mason.[20] Results obtained from the current method for the loading, the total induced drag, and the drag of the individual wings are all identical to those presented by Iglesias and Mason.[20] The details of this comparison can be found in Ref. 21.

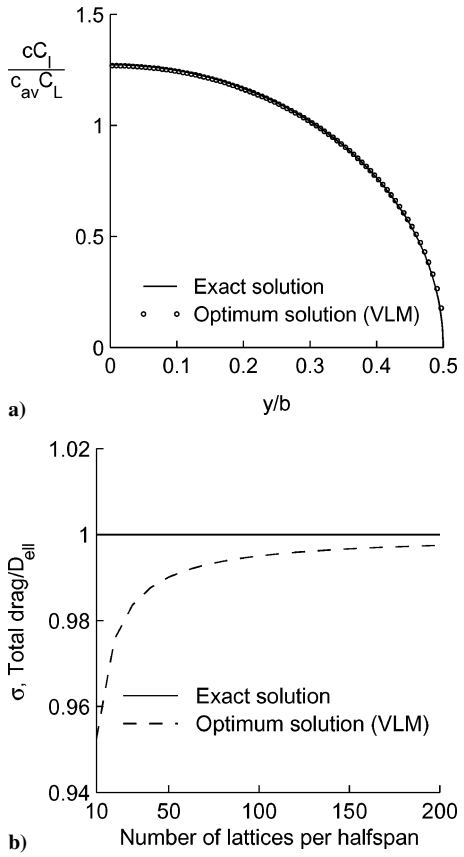

Fig. 6 Comparison of the optimal solution for a planar wing from VLM with the exact solution: a) spanload distribution and b) convergence of the predicted induced drag with increasing number of lattices per half-span.

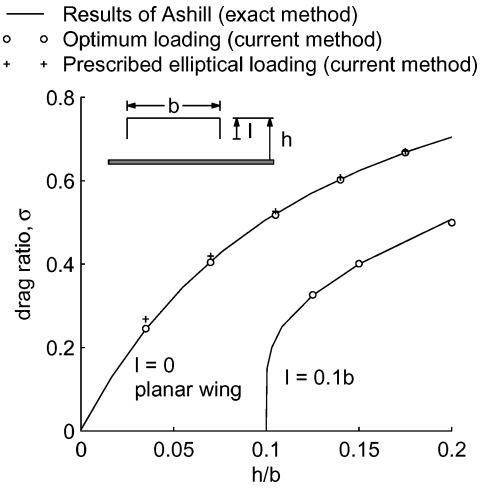

Fig. 7 Comparison of drag factors for wings in ground effect from the current method with exact solutions from Ashill.[11]

Single Wing in Ground Effect

Ashill[11] has presented an exact approach for determining the minimum induced drag of wings in ground effect. The resulting induced-drag ratios for a planar and a nonplanar wing, as calculated by the current vortex-lattice method, have been compared with Ashill's exact results. The induced drag ratio σ is the ratio of the induced drag in ground effect nondimensionalized by D_{ell} for the same lift, span, and dynamic pressure. Thus, a lower value of σ indicates a larger ground-effect benefit for the wing. Figure 7 shows a comparison of the σ computed using the current method for optimally loaded wings at various heights above ground with those from Ashill.[11] The nonplanar wing used in this comparison has a 10%-span downward-pointing winglet at each wing tip. The agreement is seen to be excellent. The results also indicate that for a given h a wing with a downward-pointing winglet experiences greater ground-effect benefits than a planar wing.

Also presented in Fig. 7 are the values of σ for the elliptically loaded planar wing, determined using the exact solution of D_{int} in Fig. 5b and Eq. (21). As seen, the elliptically loaded planar wing has nearly the same induced drag as an optimally-loaded planar wing at a given height above ground. This observation is not new; a similar comparison was presented by Ashill[11] in which the minimum-induced drag results were compared with the induced drag computed by Wieselsberger[9] for elliptically loaded wings in ground effect.

The optimum normalwash and optimum lift distributions, for both planar and nonplanar wings, are presented in Fig. 8 for various values of h. Figure 8a shows the optimum Trefftz-plane downwash distributions for the planar wing of aspect ratio 8, and Fig. 8b shows the corresponding lift distributions. The $h/b = 0.02$ case is used to illustrate an example with extreme ground effect. The resulting lift distributions agree well with the results of de Haller,[10] who showed that when the height above ground diminishes from infinity to zero, the optimal loading changes from elliptic to parabolic. Rozhdestvensky[12] found the same parabolic spanwise distribution for the optimal wing in extreme ground effect (clearances of 10% of the wing span or smaller).

The optimum normalwash distributions for the nonplanar wing, plotted in Fig. 8c as a function of the wing arc length, show that the normalwash on the winglet is exactly zero. Because of the presence of the winglet, however, the downwash on the planar portion of the wing, at a given h, is less than the downwash on the wing without a winglet. This reduced downwash caused by the winglet results in lower induced drag for the nonplanar wing when compared to a planar wing. The optimum load distributions for the nonplanar wing are presented in Fig. 8d. It is seen that with changes in h there is hardly any change to the loading on the planar portion as the changes are confined mainly to the loading on the winglet. For a wing designed to operate in ground effect at a given σ, a wing with a downward-pointing winglet might prove to be advantageous

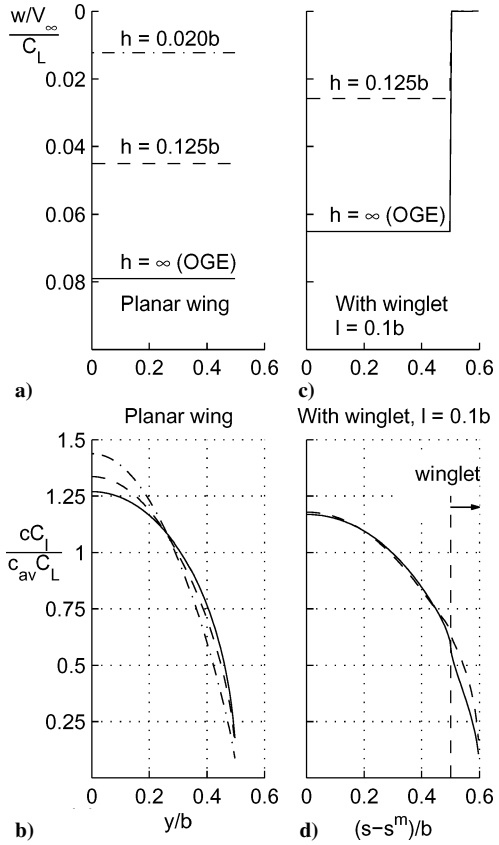

Fig. 8 Planar and nonplanar wings in ground effect at various h: a) Trefftz-plane downwash distributions for planar wings, b) spanload distributions for planar wings, c) Trefftz-plane normalwash distributions for nonplanar wings, and d) spanload distributions for nonplanar wings.

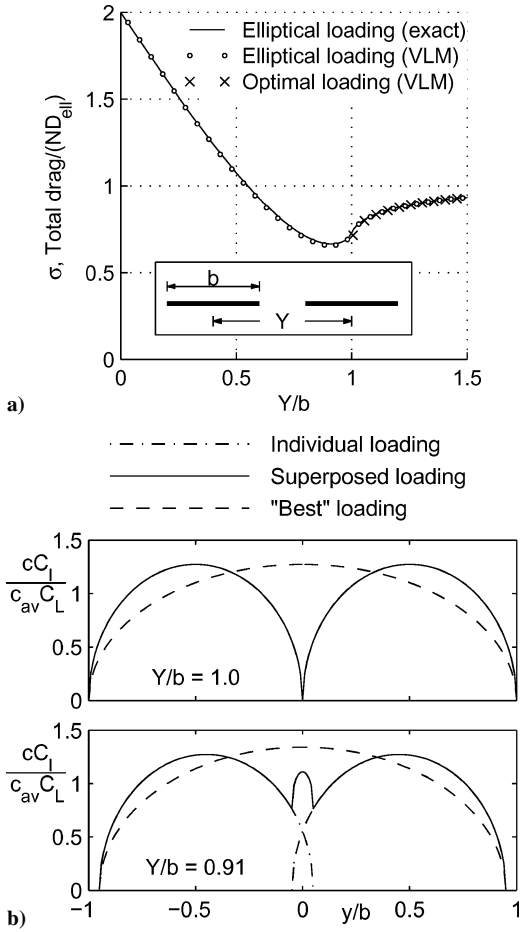

Fig. 9 Two-wing formation: a) variation of drag ratio with lateral separation for optimal and elliptical loadings, with inset showing the wake traces, and b) comparison of the superposed loading with the best loading for $Y/b = 1$ and 0.91.

because the height of the planar portion of the wing above ground is greater than that for a wing without a winglet.

Because flight safety becomes an increasingly important issue for small ground clearances, it is desirable to develop concepts for achieving ground-effect benefits at larger clearances. It can be seen from Fig. 7 that for optimally loaded and elliptically loaded planar wings, the ground-effect benefit depends on h/b. It can be deduced from these results that for achieving a given ground-effect benefit, as determined by σ, a larger-span wing can fly at a larger ground clearance h than a smaller-span wing. For example, a 50% induced-drag savings can be achieved by flying at a height of approximately 10% of the wing span above the ground. Routine flight operations at this h/b can be dangerous for a 10-m span aircraft, but starts to become conceivable for a 100-m span aircraft concept.

Results

The results presented in this section focus on three main topics: 1) the effect of lateral separation on drag benefits for formations flying OGE, 2) the benefits of combined formation and ground-effect flight, and 3) the optimal vee shapes of formations. In all cases, the wings within a given formation are all assumed to be planar with identical span b and supporting the same lift L. In the discussion of drag benefits, a comparison is made between drag ratios of different formations. For an N-wing configuration, IGE or OGE, the drag ratio σ is the ratio of total induced drag of that configuration to the induced drag of N elliptically loaded planar wings of span b, with lift L, and flying in isolation OGE at the same freestream dynamic pressure as the formation.

Effect of Lateral Separation

To analyze the effects of lateral separation on formation flight, a formation of two planar wings is used. The vertical separation Z is assumed to be zero so that the two wings lie in the same horizontal plane. Two loading cases are considered: one in which each wing is loaded optimally for minimum total induced drag, and the second in which each wing has a prescribed elliptical loading.

The variation of the drag ratio σ for this two-wing formation as a function of nondimensional lateral separation Y/b is shown in Fig. 9a for both of the two loading cases. The results for the elliptical loading are shown from the vortex-lattice approach as well as from the exact approach, and these two approaches give nearly identical results. The results for the optimal-loading case are presented only for $Y/b > 1$ as the optimum-downwash theory, as presented earlier in this paper, is not valid for computing the minimum-induced-drag loading on planar wings with overlapping or intersecting wake traces. For $Y/b > 1$, a comparison of the induced-drag-ratio variations for the two loading cases illustrates that a formation of elliptically loaded wings has virtually the same induced drag as a formation that has the theoretical optimum loading. This observation, made earlier by Lissaman and Shollenberger,[2] has an important consequence for adaptive wings that can reconfigure their geometries (such as spanwise twist or camber distribution) for formation flight. The wing geometries can be adapted to achieve an elliptical loading that is invariant with formation geometry instead of an optimal loading that will need to be recomputed depending on the formation geometry.

It is seen from Fig. 9a that for values of lateral separation ($Y/b \gg 1$) the drag ratio asymptotes to 1 because the wings have little influence on each other. For $Y/b = 1$, corresponding to zero lateral overlap, the drag ratio is 0.73, representing a 27% drag reduction when compared to the total drag of two wings flying in isolation. As the lateral separation is decreased, the drag ratio continues to decrease until a minimum in the drag ratio is reached for a lateral separation of Y/b of 0.91 that corresponds to a geometry

where there is a 9%-span lateral overlap of the wing tips. For this optimum lateral separation, the drag ratio is 0.66, which represents a 44% reduction in drag when compared to the total drag of two wings flying in isolation.

The reason for the optimum lateral separation of $Y/b = 0.91$ can be deduced from a comparison of the loadings for $Y/b = 1$ and $Y/b = 0.91$ with the corresponding "best" loadings in Fig. 9b. For any Y/b, the best loading is one that distributes the total formation lift elliptically over the formation span. The formation span is the lateral distance from the left wing tip of the left wing to the right wing tip of the right wing. For $Y/b = 1$ and 0.91, the formation spans are $2b$ and $1.91b$, respectively. Although the formation span for $Y/b = 0.91$ is less than that for $Y/b = 1$, the superposed loading is closer to the best loading for $Y/b = 0.91$ than for $Y/b = 1$. For $Y/b < 0.91$ (not shown), the superposed loading is even closer to the corresponding best loading, but the formation span is also much smaller than for $Y/b = 0.91$. As a result of this tradeoff, $Y/b = 0.91$ is the optimum lateral separation.

It is also possible to quantify the formation drag benefit by determining an effective span for the formation. This effective span b_{eff} is the span of a single elliptically loaded wing carrying the same total lift as the formation and having the same total induced drag as the formation. It can be shown that $b_{\text{eff}}/b = \sqrt{(N/\sigma)}$. For $Y/b = 0.91$, the effective span for this formation geometry is $1.73b$, implying that this two-wing formation at the optimum lateral separation behaves like a single large wing of span $1.73b$ with respect to induced-drag characteristics. For lateral separations much less than $Y/b = 0.91$, the drag ratio increases rapidly and reaches a value of 2 for $Y/b = 0$, which represents a 100% increase in the drag when compared to the total drag of two wings flying in isolation.

The 9%-span optimum lateral overlap of wing tips predicted in the current work for elliptically loaded wings is close to those seen in wind-tunnel and flight experiments. Blake and Gingras[23] presented wind-tunnel test results for two delta-wing aircraft in formation and compared wind-tunnel measurements with predictions from a vortex lattice method. Both predictions and the experimental measurements showed a trend of maximum drag reduction when there is an approximate 10–20%-span lateral overlap of wing tips in the formation. Recent experiments performed at NASA Dryden Flight Research Center[25,26] analyzed performance benefits resulting from formation flight, using two modified F/A-18 aircraft. A summary of drag-reduction results computed using actual test points shows a maximum reduction in induced drag when there is an 8–18%-span lateral overlap in wing tips and a small vertical separation of approximately 5% of the wing span.[26] Given that the theoretical model in the current work does not account for wake roll up and assumes an elliptical loading, the results for the optimum lateral overlap agree well with the trends seen in the experiments.

Combined Formation and Ground-Effect Flight

The motivation for studying the benefits of combined formation and ground-effect flight stems from two main observations, both discussed earlier: 1) a larger-span wing achieves the same ground-effect benefit (same σ) as a smaller-span wing but at a larger height above ground h, and 2) a formation at near-optimal lateral separation behaves like an effectively large-span wing with respect to induced drag. Based on these two observations, a hypothesis was made that a formation of several wings will be able to experience ground-effect benefits at larger heights than a single wing. Owing to the fact that safety issues and the demand for very precise control of h become increasingly important for flight in close proximity to the ground, it is worthwhile exploring concepts that will enable the achievement of ground-effect benefits at large values of h. With this goal, combined formation and ground-effect flight was studied, and the results are presented in this subsection.

As a first step in examining the combined effect of formation and ground-effect flight, the current method was used to determine the optimum downwash and optimum lift distributions for three planar wings flying in formation at various h. A lateral separation of $Y/b = 1.02$ along with a zero vertical separation were used for this part of the study.

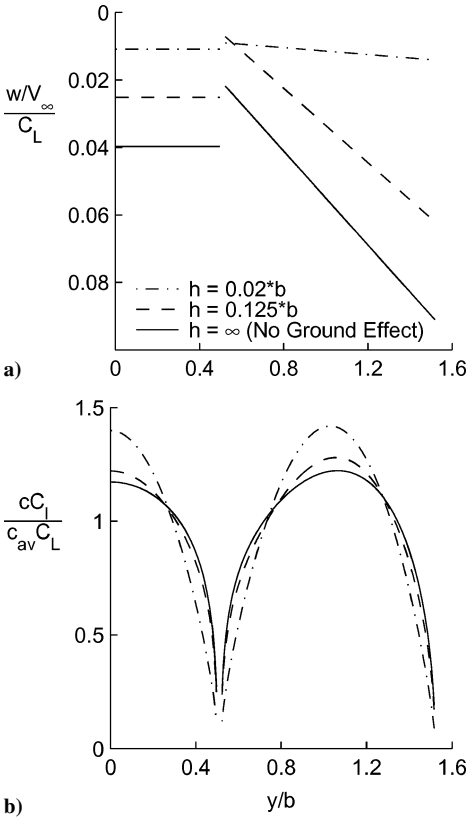

Fig. 10 Wing formation in ground effect: a) optimum Trefftz-plane downwash distributions and b) optimum spanload distributions at various h.

Figure 10a shows the resulting nondimensional Trefftz-plane downwash distributions. The $h/b = 0.02$ case is intended to represent an extreme ground-effect configuration. The linear variation of downwash across the span of each wing is clearly seen. Figure 10b shows the corresponding spanwise lift distributions on the wings. With trends similar to those observed for the single wing in ground effect, the downwash magnitude decreases with decreasing height above ground (Fig. 10a). The load distribution that is most parabolic in shape in Fig. 10b corresponds to the smallest height, $h/b = 0.02$. For this lateral separation, the spanwise downwash and lift distributions for $h/b = 0.02$ are very close to those observed for the single planar wing in ground effect shown earlier in Figs. 8a and 8b.

Although the optimal loading is noticeably different from an elliptical loading, especially for close formations and small ground clearances (Fig. 10b, $h/b = 0.02$), the drag ratios (not shown) for elliptically loaded wings in formations are nearly the same as those for the corresponding optimally loaded wing formations. For this reason, only the elliptically loaded cases are presented in the remainder of this study.

As a second step in the study of combined formation and ground-effect flight, the variations of the induced-drag ratio σ for formations of three and 25 wings as a function of lateral separation Y/b were examined for flight both in and out of ground effect. In all cases, the vertical separation between the wings was zero. The 25-wing case was selected as an example of a very large formation similar to a flock of birds in flight. For both formations, each wing was elliptically loaded, and the lateral separation was increased from $Y/b = 0$ to 2.5. For the case of flight IGE, each formation was examined at a representative height of $h/b = 0.5$.

For the three-wing formation in Fig. 11a, it can be seen that the optimum lateral separation for the formation both IGE and OGE is at $Y/b = 0.9$. At any Y/b, the σ for the IGE case of this formation is less than that for the OGE case by approximately 0.08 over the range of Y/b plotted in Fig. 11a. For the larger formation of 25 wings seen in Fig. 11b, the optimum lateral separation is nearly the same as for the three-wing formation, at $Y/b = 0.89$. At this optimum lateral

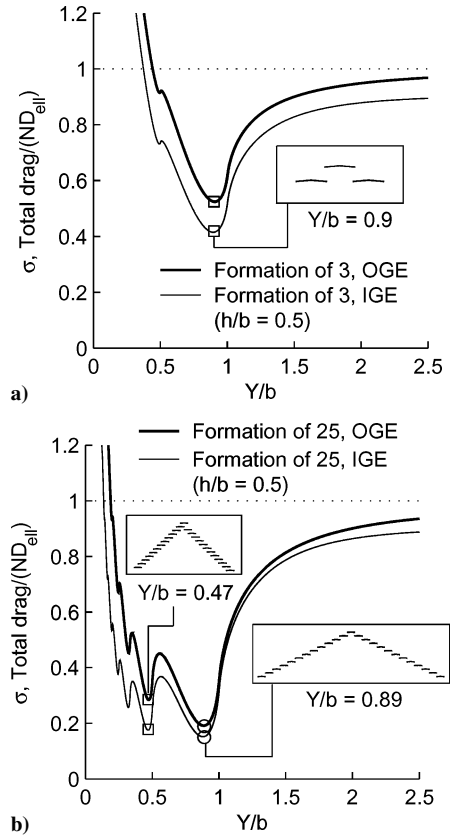

Fig. 11 Exact results for the effect of lateral separation on drag ratio for three- and 25-wing formations in and out of ground effect with insets showing the plan views of formation geometries at arbitrary streamwise spacings.

separation, the σ is 0.19, implying that the drag reduction is 81% compared to 25 wings flying in isolation out of ground effect. For both formations, it can be stated that ground effect does not influence the optimum lateral separation for the induced drag ratio. Unlike the three-wing formation, the difference in the drag ratio between the OGE and IGE cases of the 25-wing formation varies considerably with lateral separation. In particular, there is little difference in σ between the OGE and IGE cases for Y/b between 1.05 and 1.25, where adjacent wings tips are closely spaced but do not overlap. When the wing tips overlap, the difference in the σ between OGE and IGE cases increases with decreasing Y/b.

For the 25-wing formation, there are distinct multiple local minima, with the prominent second and third local minima located at $Y/b = 0.47$ and 0.32. These lateral-separation values are approximately one-half and one-third of the lateral separation of $Y/b = 0.89$ for the first minimum. These multiple local minima also occur for the IGE case at the same Y/b values. A study of the relative contributions of the different f terms in Eq. (22) can be used to explain the occurrence of these multiple local minima. The primary minimum at $Y/b = 0.89$ occurs because of strong favorable interference between every wing and its adjacent neighbor (wings i and $i+1$). The second local minimum at $Y/b = 0.47$ occurs because of strong favorable interference between pairs formed by a wing and its next-to-immediate neighbor (wings i and $i+2$). Likewise, the third local minimum occurs because of strong favorable interference between wings i and $i+3$.

Additionally, from a study of the relative contributions of the different g terms in Eq. (23), it can be seen that there is stronger favorable interference between pairs formed by a wing and the image of its adjacent neighbor for $Y/b = 0.47$ than for $Y/b = 0.9$. As a result, the σ values for the first and second minima in the IGE case differ by only 0.025. In other words, the drag difference between the two minima in the IGE case is only 2.5% of 25 D_{ell}. With increasing number of wings, the second minimum for the IGE case becomes even more pronounced. For example, for a 100-wing formation at $h/b = 0.5$, the second minimum has slightly less drag than the primary minimum. Although the drag ratio at the second minimum is close to that at the first minimum, the drag in the vicinity of this second minimum is more sensitive to the lateral separation, whereas the first minimum at $Y/b = 0.89$ is comparatively more flat. The formation plan views shown in the insets in Fig. 11b illustrate the differences in the lateral separation at the primary and secondary minima and have been shown with an arbitrary streamwise spacing between the wings. The right leg of the vee shape for $Y/b = 0.47$ has been displaced slightly downstream of the left leg to avoid collision between the two wings on either side of the lead.

Although for $Y/b < 1$ the drag-ratio variation for the 25-wing formation has considerable waviness, there is a wide range of Y/b from approximately 0.3 to 1.05 that results in at least 50% drag reduction compared to 25 wings flying solo and OGE. This large range of beneficial lateral separations and the multiple local minima for large formations can partly explain the considerable imprecision and variation in lateral separation that is observed in birds flying in formation.[8] For very small lateral separations in the OGE case, there is a steep increase with the drag ratio reaching a value of 25 for $Y/b = 0$, a value that matches the exact result from Munk's stagger theorem. More generally, it can be shown that the σ for N wings flying OGE at $Y/b = 0$ and $Z/b = 0$ is exactly N.

As a third step in the examination of combined formation and ground-effect flight, the effect of height above ground was studied for a single-wing and for wing formations. Figure 12 presents the drag ratio for a single wing and for formations of three and 25 wings in ground effect at various heights above ground. For both formations, the results have been plotted for two lateral-separation values of $Y/b = 0.9$, corresponding to the optimum lateral separation, and $Y/b = 1.1$, corresponding to a separation with no lateral overlap of wing tips. These two values have been used to further illustrate the important effects of wing-tip overlap on drag benefits. The drag ratio of each formation OGE has also been plotted, which corresponds to the asymptote as $h/b \to \infty$. For any given formation, the difference between the OGE drag ratio and the IGE drag ratio, for a certain h/b, is a measure of the ground-effect benefit for that h/b.

The drag-ratio variation for the single-wing case is the same as that shown earlier in Fig. 7 and serves as a good reference. It is seen that for small ground clearances of $h/b < 1$ the reduction in σ caused by ground effect is significant for the single-wing and for the three-wing formations. However, the reduction in σ at these clearances is comparatively marginal for the 25-wing formations. At these small ground clearances, the images of neighboring wings are in regions of adverse interference. As a result, the cumulative contribution of the g terms in Eq. (23) is adverse for large formations, and this adverse contribution detracts from the favorable effects between each wing and its own image. For large ground clearances of $h/b > 2$, the situation is reversed: large formations experience

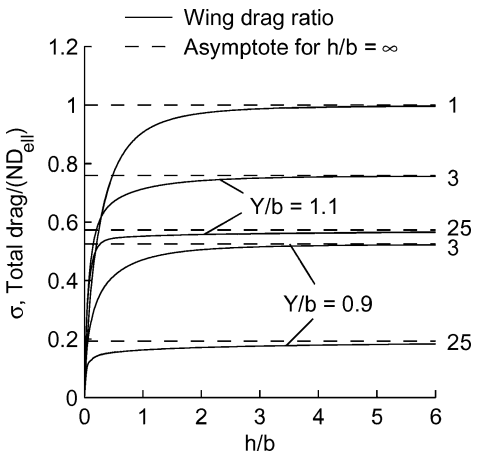

Fig. 12 Drag ratios for a single wing and for formations of three and 25 wings in ground effect.

greater reductions in σ when compared to a single-wing or smaller formations. At large ground clearances, the favorable effects between each wing and its own image diminish rapidly with increasing h/b, as seen from the results of the single-wing case. However, for large formations the cumulative effect of the images of adjacent wings become favorable because the images of neighboring wings are in regions of favorable interference. Although this effect is small, it persists even at relatively large ground clearances of $h/b \approx 4$. As a result, there is a small, but noticeable, reduction in σ for large formations even at large ground clearances, as seen for the 25-wing formations in Fig. 12. Thus, combined formation and ground-effect flight results in a small additional reduction in induced drag, even at large ground clearances, and might at least partly explain why some species of migrating birds are seen to fly in formation close to the ground.

The importance of maintaining the optimal lateral separation of approximately $Y = 0.9b$ is seen by comparing the two drag-ratio curves for the 25-wing formations in Fig. 12. For any given h/b, the formation-induced drag for $Y = 1.1b$ is almost three times that obtained with the optimum separation of $Y = 0.9b$. Thus, it is important to maintain a small lateral overlap of wing tips for large formations, whether OGE or IGE. As seen from the results of Fig. 11b, it is better to err on the smaller-Y/b side of the optimum lateral separation than on the larger-Y/b side. That is, a wide range of Y/b values that result in lateral wing-tip overlap provide greater drag reduction than nonoverlapped wings with $Y/b > 1.1$. Lateral overlap of wings does not imply that the aircraft have to fly close to each other. As pointed out by Munk's stagger theorem, the total formation-induced drag is independent of the streamwise separation between the wings as long as the spanwise lift distributions are maintained. Thus, the aircraft can be well separated in the streamwise direction for safety.

Optimal Vee-Formation Shapes

Migrating birds are often seen flying in vee-shaped formations. Of particular interest in the current study was the difference in the shape of the optimal vee formation for OGE and IGE flight. The optimum vee-formation shape was found by setting the requirement that each wing have equal induced drag. Figure 13a shows the resulting optimum formations for a formation of 25 wings IGE and OGE. A lateral separation of $Y/b = 0.9$ with zero vertical separation was used. A clearance of $h/b = 1.0$ was used for ground-effect flight. The optimal shape of the vee formation is not an exact "V", but a shape that is more swept at the tips and rounded at the apex. Similar optimal vee-formation shapes were reported by Lissaman and Shollenberger[2] and by Hummel.[4] The differences in formation shape in and out of ground effect are insignificant, indicating that the optimum vee shape for the formation OGE would serve just as well for the formation IGE. The results in Fig. 13a show that, for equipartition of drag, the wings near the apex of the vee are very closely spaced. Such close separation might not be practical for routine aircraft flight operations. Thus, it might be necessary to compromise on the equipartition of drag in order to decrease the risk of collision. Additionally, the exact shape of this vee formation might not be correct for bird formations, where the flapping frequency of the wings can have an additional effect on longitudinal separation.

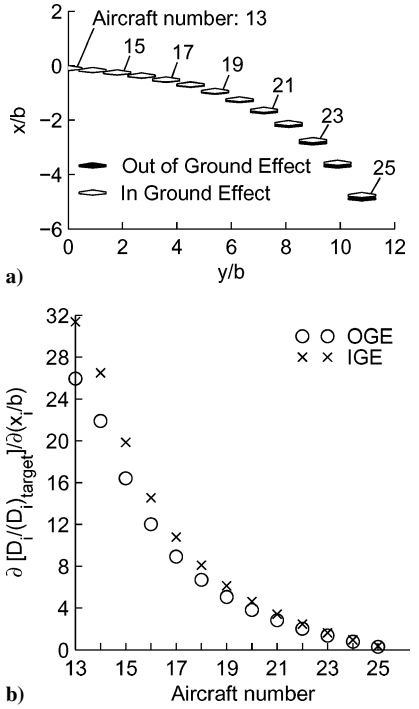

Fig. 13 Optimum vee-formation shapes: a) 25-wing formation in and out of ground effect ($h/b = 1$) and b) gradient of individual induced drag with streamwise location for a formation of 25 wings in and out of ground effect ($h/b = 1$).

It was of interest to determine the natural stability of the streamwise position of each individual in the formation, to see if the vee formation is a natural and stable flight mode. This stability was determined by examining the variation of the individual induced drag with streamwise location. Figure 13b is a plot of the gradient of individual induced drag (nondimensionalized by the target individual induced drag for the optimum vee formation) with respect to streamwise location for each wing on the right-hand side of the vee formation. The wings are numbered from 13 to 25, with wing 13 denoting the one at the apex of the vee formation, and wing 25 denoting that at the right tip of the formation. Lissaman and Shollenberger[2] observed that if a bird moves ahead of the vee formation, more power is required for it to maintain the same airspeed, and when flying aft of the vee formation less power is required. In either case, the bird will tend to return to its original position within the vee formation. This result is confirmed in the current work by the fact that the gradients in Fig. 13b are positive for all wings, with positive x pointing in the direction of flight. The differences in gradients between the OGE and IGE cases are small, indicating that ground effect does not significantly affect the position stability.

For an aircraft flying at the tips of the formation, however, changes in streamwise location do not result in significant changes in induced drag, as seen in Fig. 13b. With gradients approaching zero, the aircraft located at the tip of the formation will find it more difficult to maintain position in formation. Weimerskirch and colleagues[7] witnessed this behavior during the experiments conducted on a formation of great white pelicans and state that pelicans often had difficulty staying within formation when flying at the tips.

Conclusions

The objective of this work was to examine the induced-drag benefits of formation flight both in and out of ground effect. The theoretical models used in this research assume rigid, inviscid wakes that trail without roll up in the downstream direction. The wings in the current work were all loaded ideally in one of two ways: with an optimum lift distribution or with an elliptical lift distribution. The optimum lift distribution results in a minimum for the total induced drag of the formation while satisfying constraints on the lift and rolling moment on each wing. The resulting induced drag represents the lowest limit attainable for a given formation and ground-effect configuration. For determining the optimum lift distribution, an optimum-downwash-based approach using a vortex lattice implementation was used. This method, however, is valid only for formations in which there is no overlap of the wake traces for the wings. For the cases with elliptically loaded planar wings, it was possible to develop an exact approach for formations in or out of ground effect. This exact approach is applicable to cases with or without lateral overlap of wings. For this exact approach, the exact interference-drag solution for a two-aircraft problem was first developed, which was helpful in identifying regions of favorable and adverse interference. For a formation of several wings, in or out of ground effect, the total drag was decomposed into the self-induced contributions and the mutual-induced terms for the different aircraft pairs. Each of these mutual-induced terms was determined from the two-aircraft interference solution.

A comparison of optimally loaded and elliptically loaded planar wings showed that, for any formation or ground-effect configuration, the two loading scenarios resulted in virtually the same total drag. The benefit of using elliptical loading instead of optimal loading is that the target loading for each wing is independent of the formation geometry or height above ground. To generate the target lift distribution, however, there is a need for an appropriate twist or camber variation across the span of each wing. Because this spanwise geometry variation is dependent on the formation configuration and ground clearance, the wing geometry will need to adapt its shape, much like that of a bird.

For any formation of planar wings at any ground clearance, the optimum lateral separation between adjacent wings corresponds to a lateral overlap of approximately 10% of the wing span. At this optimum lateral separation, the favorable interference between adjacent wings is maximized. This optimum lateral separation is close to that observed in wind-tunnel and flight experiments. For large formations, multiple local minima were observed in the drag variation with lateral spacing. These multiple local minima were shown to occur because of the variations in interference drag between each wing and its successive neighbors. For large formations in ground effect, it was shown that the lateral separations corresponding to the primary and secondary local minima resulted in nearly the same drag. The presence of these local minima with nearly the same drag might explain the considerable variations and imprecision in lateral separation that are often observed in bird formations.

The results for combined formation and ground-effect flight show that large formations are able to achieve a small, but noticeable, benefit caused by ground effect even at a relatively large ground height of four wing spans. When the streamwise separation is adjusted for equal distribution of the drag benefit among all of the wings in a formation, a vee-shaped formation results. This vee-formation shape is practically independent of the ground clearance. When flying in such a vee formation, the sensitivity of the individual-aircraft drag as a result of changes to the streamwise position provides automatic streamwise-position stability for the aircraft. This stability is highest for the lead aircraft and degrades toward the tips of the vee formation, which supports observations made by other researchers that pelicans located at the tips of a vee-shaped formation often have difficulty maintaining their position.

With the potential for achieving dramatic improvements in aircraft performance, formation and ground-effect flight techniques hold significant promise for use in future aeronautical systems. It is believed that this research provides valuable insight into the aerodynamics of formation and ground-effect flight by a quantification of the benefits for ideally loaded wings in configurations that maximize the favorable interference between the wings.

Acknowledgments

The authors would like to express gratitude for the funding provided by the Frank C. Ziglar, Jr. Endowed Graduate Fellowship for the first author. Peter Lissaman is thanked for several helpful discussions on this work and for his encouragement regarding the development of the exact solution. Blaine Rawdon is thanked for suggesting the examination of nonplanar wings in ground effect. The authors also thank the reviewers for their comments which have helped improve the paper.

References

[1]Wieselsberger, C., "Beitrag zur Erklärung des Winkelfluges einiger Zugvögel," *Zeitschrift für Flugtechnik und Motorluftschifffahrt*, Vol. 5, 1914, pp. 225–229.

[2]Lissaman, P. B. S., and Shollenberger, C. A., "Formation Flight of Birds," *Science*, Vol. 168, No. 3934, 1970, pp. 1003–1005.

[3]Hummel, D., "Aerodynamic Aspects of Formation Flight in Birds," *Journal of Theoretical Biology*, Vol. 104, No. 3, 1983, pp. 321–347.

[4]Hummel, D., "Formation Flight as an Energy-Saving Mechanism," *Israel Journal of Zoology*, Vol. 41, No. 3, 1995, pp. 261–278.

[5]Hummel, D., "The Use of Aircraft Wakes to Achieve Power Reductions in Formation Flight." AGARD CP-584, May 1996.

[6]Hainsworth, F. R., "Precision and Dynamics of Positioning by Canada Geese Flying in Formation," *Journal of Experimental Biology*, Vol. 128, No. 1, 1987, pp. 445–462.

[7]Weimerskirch, H., Martin, J., Clerquin, Y., Alexandre, P., and Jiraskova, S., "Energy Saving in Flight Formation," *Nature*, Vol. 413, No. 6857, 2001, pp. 697, 698.

[8]Hainsworth, F. R., "Induced Drag Savings from Ground Effect and Formation Flight in Brown Pelicans," *Journal of Experimental Biology*, Vol. 135, No. 1, 1988, pp. 431–444.

[9]Wieselsberger, C., "Uber den Flugwiderstand in der Nahe des Boden," *Zeitschrift für Flugtechnik und Motorluftschifffahrt*, Vol. 10, 1921, p. 145.

[10]de Haller, P., "La Portance et la Traine Induite Minimum d'une Aile au Voisinage du Sol," Mitteilungen aus den Institut fur Aerodynamick, Zurich, Vol. 5, 1936.

[11]Ashill, P. R., "On the Minimum Induced Drag of Ground Effect Wings," *Aeronautical Quarterly*, Vol. XXI, Aug. 1970, pp. 211–232.

[12]Rozhdestvensky, K. V., *Aerodynamics of a Lifting System in Extreme Ground Effect*, Springer-Verlag, New York, 2000.

[13]Katz, J., and Plotkin, A., *Low-Speed Aerodynamics*, Cambridge Aerospace Series, Cambridge Univ. Press, Cambridge, England, U.K., 2001, Chap. 12.

[14]Reid, E. G., "A Full-Scale Investigation of Ground Effect," NACA Rept. 265, 1928.

[15]Curry, R. E., and Bowers, A. H., "Ground-Effect Analysis of a Jet Transport Airplane," NASA TM 85920, Jan. 1985.

[16]Curry, R. E., Moulton, B. J., and Kresse, J., "An In-Flight Investigation of Ground Effect on a Forward-Swept Wing Airplane," NASA TM 101708, Sept. 1989.

[17]Rayner, J. M. V., "On the Aerodynamics of Animal Flight in Ground Effect," *Philosophical Transactions of the Royal Society of London B*, Vol. 334, No. 1269, 1991, pp. 119–128.

[18]Feifel, W. M., "Optimization and Design of Three-Dimensional Aerodynamic Configurations of Arbitrary Shape by a Vortex Lattice Method," NASA SP 405, May 1976, pp. 71–88.

[19]Beukenberg, M., and Hummel, D., "Aerodynamics, Performance and Control of Airplanes in Formation Flight," International Council of the Aeronautical Sciences, ICAS 90-5.9.3, Sept. 1990.

[20]Iglesias, S., and Mason, W. H., "Optimum Spanloads in Formation Flight," AIAA Paper 2002-0258, Jan. 2002.

[21]Frazier, J. W., and Gopalarathnam, A., "Optimum Downwash Behind Wings in Formation Flight," *Journal of Aircraft*, Vol. 40, No. 4, 2003, pp. 799–803.

[22]Gingras, D. R., Player, J. L., and Blake, W. B., "Static and Dynamic Wind Tunnel Testing of Air Vehicles in Close Proximity," AIAA Paper 2001-4137, Aug. 2001.

[23]Blake, W. B., and Gingras, D. R., "Comparison of Predicted and Measured Formation Flight Interference Effects," *Journal of Aircraft*, Vol. 41, No. 2, 2004, pp. 201–207.

[24]Wagner, G., Jacques, D., Blake, W., and Pachter, M., "Flight Test Results of Close Formation Flight for Fuel Savings," AIAA Paper 2002-4490, Aug. 2002.

[25]Vachon, M. J., Ray, R. J., Walsh, K. R., and Ennix, K., "F/A-18 Aircraft Performance Benefits Measured During the Autonomous Formation Flight Project," AIAA Paper 2002-4491, Aug. 2002.

[26]Ray, R. J., Cobleigh, B. R., Vachon, M. J., and John, C. S., "Flight Test Techniques Used to Evaluate Performance Benefits During Formation Flight," AIAA Paper 2002-4492, Aug. 2002.

[27]Laurenzo, R., "A Long Wait for Big Wigs," *Aerospace America*, Vol. 41, No. 6, 2003, pp. 36–40.

[28]Kroo, I., "Innovations in Aeronautics," AIAA Paper 2004-0001, Jan. 2004.

[29]McMasters, J. H., and McLean, J. D., "The Formation Flight of Human Powered Aircraft Across the English Channel in the Spring," *Swiss Aero Revue*, Dec. 1979; also XVIth Congress of the Organization Scientifique et Technique International du Vol-a-Voilé (OSTIV), Château roux, France, 1978.

[30]Kroo, I. M., "A General Approach to Multiple Lifting Surface Design and Analysis," AIAA Paper 84-2507, Oct. 1984.

[31]Grasmeyer, J., "A Discrete Vortex Method for Calculating the Minimum Induced Drag and Optimum Load Distribution for Aircraft Configurations with Noncoplanar Surfaces," VPI-AOE-242, Virginia Polytechnic Inst. and State Univ., Blacksburg, VA, Jan. 1997.

[32]Stanewsky, E., "Aerodynamic Benefits of Adaptive Wing Technology," *Aerospace Science and Technology*, Vol. 4, No. 7, 2000, pp. 439–452.

[33]Monner, H. P., Breitbach, E., Bein, T., and Hanselka, H., "Design Aspects of the Adaptive Wing—the Elastic Trailing Edge and the Local Spoiler Bump," *The Aeronautical Journal*, Vol. 104, Feb. 2000, pp. 89–95.

[34]Kroo, I., "Drag due to Lift: Concepts for Prediction and Reduction," *Annual Review of Fluid Mechanics*, Vol. 33, 2001, pp. 587–617.

[35]Iannotta, B., "Vortex Draws Flight Research Forward," *Aerospace America*, Vol. 40, No. 3, 2002, pp. 26–30.

[36]Grosser, M., *Gossamer Odyssey*, Houghton Mifflin Co., Boston, 1981.
[37]Burke, J. D., "The Gossamer Condor and Albatross: A Case Study in Aircraft Design," AeroVironment, Inc., Pasadena, CA, Rept. AV-R-80/540, June 1980.
[38]Jones, R. T., "The Spanwise Distribution of Lift For Minimum Induced Drag of Wings Having a Given Lift and a Given Bending Moment," NACA TN 2249, Dec. 1950.
[39]Blackwell, J. A., Jr., "Numerical Method to Calculate the Induced Drag or Optimum Loading for Arbitrary Non-Planar Aircraft," NASA SP 405, May 1976, pp. 49–70.
[40]Glauert, H., *The Elements of Aerofoil and Airscrew Theory*, Cambridge Univ. Press, Cambridge, England, U.K., 1930.
[41]von Kármán, Th., and Burgers, J. M., *General Aerodynamic Theory—Perfect Fluids, Aerodynamic Theory*, Vol. 2, Julius Springer, 1935.
[42]Prandtl, L., "Induced Drag of Multiplanes," NACA TN 182, March 1924.
[43]*Symbolic Math Toolbox for Matlab: User's Guide*, The MathWorks, Inc., Natick, MA, 2004.
[44]Munk, M. M., "The Minimum Induced Drag of Aerofoils," NACA Rept. 121, 1921.
[45]King, R. M., and Gopalarathnam, A., "Ideal Aerodynamics of Ground-Effect and Formation Flight," AIAA Paper 2004-0906, Jan. 2004.